metals

MDPI

Article

Heterogeneous Nucleation and Grain Initiation on a Single Substrate

Zhongyun Fan* and Hua Men

BCAST, Brunel University London, Uxbridge, Middlesex UB8 3Ph, UK

* Correspondence: author: zhongyun.fan@brunel.ac.uk

Abstract: Recently we have proposed a new framework for early stages solidification, in which heterogeneous nucleation and grain initiation have been treated as separate processes. In this paper, we extend our atomic level understanding of heterogeneous nucleation to spherical cap formation for grain initiation on a single substrate using molecular dynamics calculations. We first show that heterogeneous nucleation can be generally described as a 3-layer mechanism to generate a 2-dimensional (2D) nucleus under a variety of atomic arrangements at the solid/substrate interface. We then introduce atomistic concept of spherical cap formation at different grain initiation undercoolings (ΔT_{gi}) relative to nucleation undercooling (ΔT_n). When $\Delta T_n < \Delta T_{gi}$, the spherical cap formation is constrained by the curvature of the liquid/solid interface, produces a dormant cap and further growth is only made possible by increasing undercooling to overcome an energy barrier. However, when $\Delta T_n > \Delta T_{gi}$, spherical cap formation becomes barrierless and undergoes 3 distinctive stages: heterogeneous nucleation to produce a 2D nucleus with radius, r_n; unconstrained growth to deliver a hemisphere of r_N (substrate radius); and spherical growth beyond r_N. This is followed by a theoretical analysis of the 3-layer nucleation mechanism, to bridge between 3-layer nucleation, grain initiation and classical nucleation theory.

Keywords: Heterogeneous nucleation; Grain initiation; MD simulation; Interface; Growth

Citation: Fan, Z.; Men, H. Heterogeneous Nucleation and Grain Initiation on a Single Substrate. *Metals* **2022**, *11*, x. https://doi.org/10.3390/xxxxx

Academic Editor(s):

Received: date
Accepted: date
Published: date

1. Introduction

Nucleation in its widest sense occurs in nearly all the technological and natural processes [1,2]. Therefore, understanding and controlling of nucleation play a critical role in advancing sciences and developing technologies. However, our current understanding of nucleation has been dominated by the classical nucleation theory (CNT) for over a century [1] with little progress of significance being made [3]. It is very desirable to see a breakthrough from this bottleneck of scientific advance and technological development.

The CNT was postulated over a century ago. Based on Gibb's ideas of nucleation [4], the first complete theory of homogeneous nucleation was formulated by Volmer and Weber [5], improved by Becker and Döring [6], and further improved by Zeldovich [7]. The homogeneous CNT was extended to heterogeneous nucleation later (see reviews in Refs. 1, 2, 8). In the homogeneous CNT, an embryo of the solid (S) of radius r is formed in the liquid (L) through structural fluctuation and a liquid/solid (L/S) interface is created as a by-product (Figure 1(a)) [1]. Based on its capillarity approximation, the homogeneous CNT applies continuum thermodynamics to determine the critical nucleus size (r^*) and the energy barrier for its formation (ΔG^*_{Hom}) through balancing the volume term and the interfacial term (Figure 1(c)):

$$\Delta G_n = \frac{4\pi}{3} r^3 \Delta G_v + 4\pi r^2 \gamma_{LS} \quad (1)$$

where ΔG_n is the total free energy change during nucleation, ΔG_v is the free energy change per volume due to solidification, and γ_{LS} is the interfacial energy of the liquid/solid (L/S) interface. Through first order differentiation one has:

$$r^* = \frac{2\gamma_{LS}}{\Delta G^*} \quad (2)$$

$$\Delta G^*_{Hom} = \frac{16\pi}{3}\frac{\gamma^3_{LS}}{\Delta G_v^2}. \quad (3)$$

In the heterogeneous CNT, a spherical cap of the solid (S) is formed on a substrate (N) with a contact angle θ defined by the Young's equation (Figure 1(b)):

$$\gamma_{LN} = \gamma_{SN} + \gamma_{LS}\cos\theta \quad (4)$$

where γ_{LN} is the interfacial energy for the liquid/substrate (L/N) interface, and γ_{SN} is the interfacial energy for the solid/substrate (S/N) interface. Although the critical radius of the nucleus (r^*) is the same for the homogeneous and heterogeneous nucleation given by Eq. 2, the energy barrier for heterogeneous nucleation (ΔG^*_{Het}) is only a fraction of that for homogeneous nucleation (Figure 1(c)):

$$\Delta G^*_{Het} = \Delta G^*_{Hom} f(\theta) \quad (5)$$

$$f(\theta) = \frac{1}{4}(2 - 3\cos\theta + \cos^3\theta). \quad (6)$$

It is important to note that θ is meaningfully defined only when $\gamma_{LN} \leq \gamma_{SN} + \gamma_{LS}$.

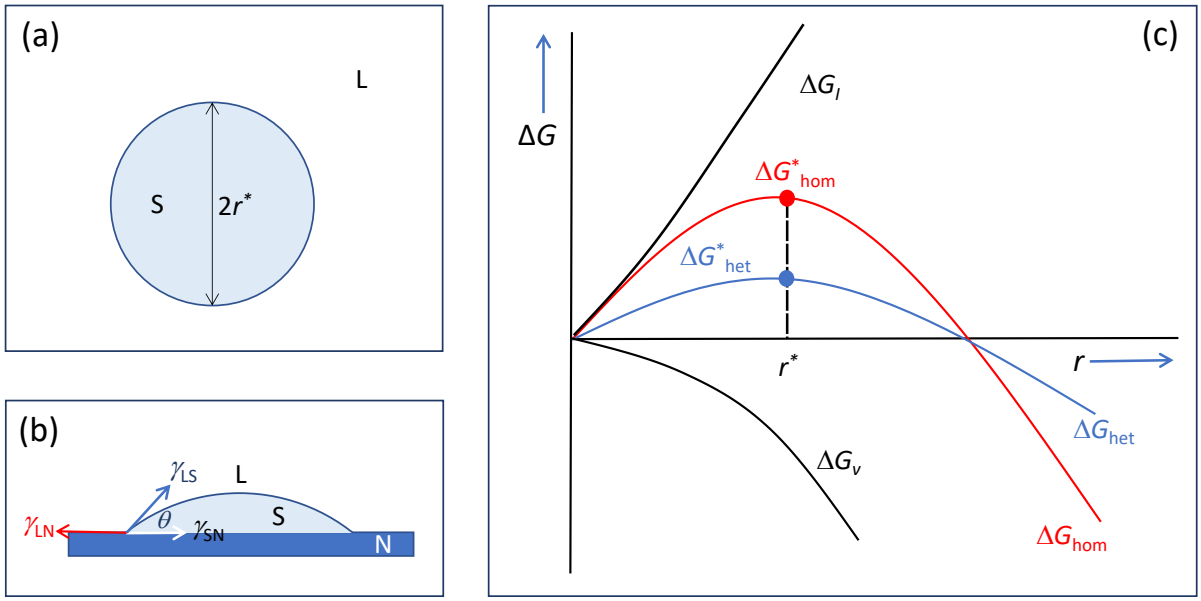

Figure 1. Schematic illustration of the classical nucleation theory (CNT). (a) Formation of the spherical nucleus of the solid (S) with a critical radius of r^* from the liquid (L) during homogeneous nucleation; (b) formation of spherical solid cap on a substrate (N) with a wetting angle of θ during heterogeneous nucleation; and (c) free energy change (ΔG) as a function of cluster size (r) showing the formation of nuclei (r^*) during homogeneous and heterogeneous nucleation processes by overcoming the energy barriers (ΔG^*_{hom}, ΔG^*_{het}) which is a consequence of balancing the interfacial energy change (ΔG_i) and volume free energy change (ΔG_v).

The homogeneous CNT is conceptually simple, mathematically rigorous, and widely applied to describe qualitatively many phase transformations and has dominated our thinking for more than a century. However, the spherical cap model of the heterogeneous CNT has been facing difficulties while dealing with cases of most interests, where the contact angle θ is small. Conceptually, the spherical cap model breaks down when $\theta \leq 10°$ since the cap height would be less than one atomic layer thick [8]. In addition, Cantor and co-works [9-12] investigated the undercooling required for the onset of solidification in the entrained liquid droplets. They found that when $\theta \geq 40°$ (corresponding to $\Delta T > 50$ K), the spherical cap model provides a reasonable fit to the observed kinetics [9, 10], while $\theta < 40°$ the spherical cap model is unable to fit the experimentally observed kinetics with

reasonable parameters [11, 12]. As early as 1934 Stranski [13] realised that for heterogeneous nucleation in systems with small θ it is better to be described as formation of monolayer disks rather than spherical caps. Richard [14] suggested that such a crystalline disk might be formed through adsorption on the substrate surface. Coudurier et al. [15] later proposed that heterogeneous nucleation might be treated as adsorption of a solid layer on the substrate, and this approach was considered by Cantor and Kim [16, 17] to interpret their results from entrained droplets. Furthermore, this solid layer approach was further extended in the so called hypernucleation theory by Jones [18, 19], where the formation of a quasi-solid layer on the TiB_2 substrate surface is envisaged to be possible even above the alloy liquidus. This insightful hypothesis has now been validated by experimental observations using the state-of-the-art electron microscopy in many cases, such as segregation of Ti, Zr, Si and Cu at the Al/TiB_2 interface [20-22], Y, Ca, and Sn at the Mg/MgO interface [23], and Y and La at the Al/Al_2O_3 interface [24]. More importantly, the general existence of ordered atoms at the liquid/substrate interface has been confirmed by atomistic simulations [3,25-27], which has been described as substrate induced atomic ordering at the liquid/substrate interface, or more generally named as prenucleation [25].

For nucleation systems involving potent substrate (i.e., small nucleation undercooling), Greer et al. [28] made the connection between the substrate radius (r_N) and the critical radius of nucleus (r^*) in CNT and developed the free growth criterion based on Eq. 2:

$$\Delta T_{gi} = \frac{2\gamma_{LS}}{\Delta S_v r_N}, \quad (7)$$

where ΔT_{gi} is the grain initiation undercooling for free growth, and ΔS_v is the entropy change of fusion per unit volume. Considering the Gibbs-Thompson coefficient $\Gamma = \gamma_{LS}/\Delta S_v$, one has:

$$\Delta T_{gi} r_N = 2\Gamma. \quad (8)$$

Free growth has been treated as effective nucleation [28, 29], and has been successfully used to predict grain size of solidified microstructures by several researchers [30-34]. In addition, one of the interesting implications of the free growth criterion is the formation of dormant spherical caps, which has now been confirmed by Gránásy and co-workers [35] through phase field crystal modelling and by Fujinaga and Shibuta [36] with large scale *molecular dynamics (*MD) simulations.

In the recent years, Fan and co-workers [3,25,37-40] have proposed a new framework for understanding early stages of solidification, in which the initial stages of formation of the solid on a substrate is defined as heterogeneous nucleation to generate a 2D nucleus [3], while the subsequent growth through spherical cap formation is treated as grain initiation [38]. Although this separation of heterogeneous nucleation from grain initiation is completely different from the conventional treatment of the subject, it may hold the potential to unify the different schools of thoughts on the subject. In addition, to understand the collective grain initiation behaviour of a population of nucleant particles we have identified two distinctive modes of grain initiation: progressive and explosive [39], which has successfully led to the development of both grain initiation maps and grain refinement maps [39,40].

The objective of this paper is to extend our atomic level understanding of heterogeneous nucleation to spherical cap formation for grain initiation on a single substrate using molecular dynamics calculations. We will start with an overview of the 3-layer nucleation mechanisms under a variety of atomic arrangements at the solid/substrate interface. We then introduce the atomistic concept of spherical cap formation at different undercoolings relative to the nucleation undercooling, i.e., constrained and unconstrained spherical cap formations. This is followed by a theoretical analysis of the 3-layer nucleation mechanism, with the intention to bridge between the 3-layer nucleation, grain initiation and classical nucleation theory.

2. Simulation approaches

A generic system was created to simulate heterogeneous nucleation process to make the simulation results generally applicable. This generic nucleation system consists of a generic liquid and a generic fcc substrate with a <111> surface orientation, with the z axis being normal to the {111} plane of the substrate. We chose aluminium as the generic liquid as it is representative of many simple metals in terms of liquid structures. The generic fcc substrate lattice was built using pinned aluminium atoms with a specified lattice parameter to pre-set the lattice misfit [25]. This generic system has two major advantages: (1) it allows the simulation of nucleation systems with substrates with high melting temperatures (T_l) that are similar to the nucleant particles used in industrial practice (*e.g.*, TiB_2 with T_l = 3498 K) and (2) this makes it possible to simulate the effect of lattice misfit alone without interference from the chemical interaction between the liquid and the substrate and/or the substrate surface roughness at atomic level [41,42]. For simplicity, we have used the generic terms "the liquid" and "the substrate" in this paper.

We used a variety of simulation systems with varying simulation cell sizes, being from 5040 to 80000. Since the melting temperature (T_m) may change slightly with the size of the simulation systems, in this paper we only use undercooling (ΔT) as an indicator of temperature, and $\Delta T = T_m - T$.

Periodic boundary conditions were imposed in the $x([11\bar{2}])$- and $y([\bar{1}10])$-directions. A vacuum region was inserted with periodic boundary conditions in the z-direction, and the extent of the vacuum region was 60 Å. The initial configuration of the fcc materials has a lattice parameter a = 4.126 Å, which corresponds to the value for aluminium obtained at its calculated melting point. The substrate was assigned to a varied lattice misfit with the solid aluminium, both negative and positive.

The EAM (embedded atom method) potential for aluminium, developed by Zope and Mishin to model interatomic interactions [43], was used in this work. The predicted melting temperature for pure Al is 870 ± 4 K with this potential [43]. During the simulation, the liquid atoms above the substrate were allowed to move freely under the effect of the interatomic potential. The substrate atoms were excluded from the equations of motion, but the forces they exert on the adjacent atoms were included. All the MD simulations were performed using the DL_POLY_4.08 MD package [44]. The equations of motion were integrated by means of the Verlet algorithm with a time step of 0.001 ps and the Berendsen NVT ensemble was used for the temperature control. The liquid was prepared by heating the system to a temperature of 1400 K with steps of 50 K, each lasting 100,000 MD steps.

The nucleation temperature, T_n, for each specified nucleation system was determined using the variable step search method. The equilibrated configuration of the liquid at 1400 K was cooled to a desired temperature with a step of 50 K and at each temperature step the system was allowed to run for 1,000,000 MD time steps to equilibrate. The initial nucleation temperature, T_1, was determined by monitoring variation in total energy and trajectory of the system during the equilibration. This means that exact nucleation occurred in the temperature interval between T_1 and T_1 + 50 K. A more accurate nucleation temperature, T_2, was determined by a finer search in this reduced temperature interval with a temperature step of 5 K. Finally, the nucleation temperature, T_n, was determined by an even finer search between T_2 and T_2 + 5 K with a temperature step of 1 K. This approach allows the nucleation temperature to be determined within an error of ±1 K.

The atomic arrangement in the liquid adjacent to the interface during the simulation is characterized by the time-averaged atomic positions [45] and local bond-order analysis [46]. The time-averaged atomic positions in the individual layers of the liquid within 10 ps were taken from the trajectory of the simulation. With this approach, the solid atoms can be distinguished from the liquid atoms, where the solid atoms usually vibrate at their equilibrium positions and the liquid atoms can move more than one atomic spacing [45]. The local bond-order analysis is another approach widely used in atomistic simulations to distinguish the solid atoms from the liquid atoms in the bulk liquid [47]. To perform the local bond-order analysis, the local bond-order parameter, $\boldsymbol{q}_l(i)$, was calculated as: [46]

$$\boldsymbol{q}_l(i) = \left(\frac{4\pi}{2l+1}\sum_{m=-l}^{l}|\boldsymbol{q}_{lm}(i)|^2\right)^{1/2}, \quad (9)$$

where the (2*l*+1) dimensional complex vector $\boldsymbol{q}_{lm}(i)$ is the sum of spherical harmonics, $Y_{lm}(r_{ij})$, over all the nearest neighbouring atoms of the atom *i*. Two neighbouring atoms *i* and *j* can be recognized to be connected if the correlation function, $\boldsymbol{q}_6(i)\cdot\boldsymbol{q}_6(j)$, of the vector $\boldsymbol{q}_6$ of neighbouring atoms *i* and *j* exceeds a certain threshold, 0.1 in this study. To distinguish the solid atoms from the liquid atoms, a threshold on the number of connections that an atom has with its neighbours is set to 6.

3. Heterogeneous nucleation on a single substrate

3.1. 3-layer nucleation mechanism

The recent advance in understanding of early stages of solidification [3,25,37-40] has led to new definitions for prenucleation [25], heterogeneous nucleation [3] and grain initiation [39,40]. Prenucleation refers to the phenomenon of atomic ordering in the liquid adjacent to a crystalline substrate. The outcome of prenucleation is a precursor for the subsequent heterogeneous nucleation, which has the highest atomic ordering and the lowest liquid/substrate interfacial energy prior to nucleation. Upon realising that the essential mechanism for both heterogeneous nucleation and crystal growth is structural templating [3,38], we have redefined heterogenous nucleation as a process that creates a 2D nucleus with a radius of r_n (effectively a crystal plane of the solid) that can template further growth [3]. Further growth of the solid proceeds by spherical cap formation although an energy barrier may exist for free growth (see Figure 2). More importantly, we found that heterogeneous nucleation completes within the first 3 atomic layers, with the 3rd layer being the 2D nucleus [3,26,27] (Figure 3). In this section, we describe briefly the 3-layer mechanism for heterogeneous nucleation under different interfacial conditions in terms of atomic matching across the solid (S)/substrate (N) interface (the S/N interface).

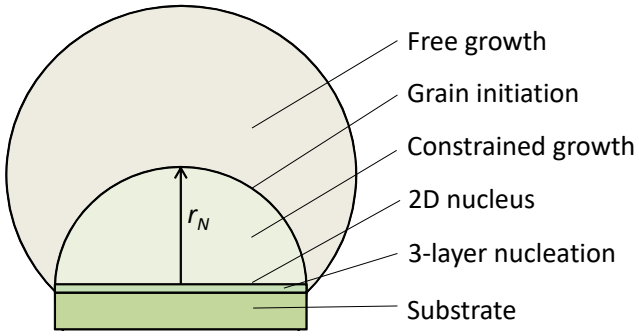

Figure 2. Schematic illustration of early stages of solidification processes on a single substrate. Heterogeneous nucleation through the 3-layer nucleation mechanism delivers a 2D nucleus. However, further growth is constrained by the curvature of the liquid/solid interface and can only occur by increasing undercooling. Grain initiation is completed by growing the solid beyond the hemisphere where free growth is possible isothermally.

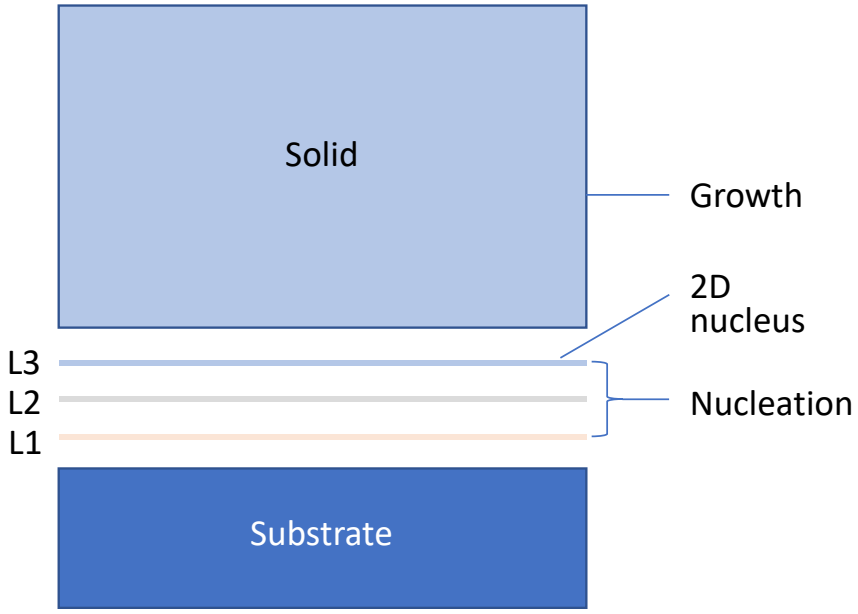

Figure 3. Schematic illustration of the 3-layer nucleation mechanism. At the nucleation temperature, heterogeneous nucleation starts with a precursor created by prenucleation, proceeds layer-by-layer through a structural templating mechanism, and completes within 3 atomic layers (marked as L1, L2 and L3) to provide a 2D nucleus (a crystal plane of the solid) which can template further growth of the solid.

Our atomistic investigation using MD simulations has established a 3-layer nucleation mechanism [38]. We found that building on the precursor created by the prenucleation process heterogeneous nucleation proceeds layer-by-layer and completes within the first 3 layers to provide a 2D nucleus. Depending on the nature of lattice misfit between the solid and the substrate, different mechanisms are operational for accommodating the misfit: dislocation mechanism for systems with small negative misfit ($-12.5\% < f < 0$); vacancy mechanism for systems with small positive misfit ($0 < f < 12.5\%$); and formation of a coincidence site lattice (CSL) as the new substrate at the stage of prenucleation for the systems with large misfit to reduce the misfit to $|f| < 12.5\%$ and then follow the mechanisms for systems of small misfit.

3.2. Effect of substrate size

Our earlier MD simulations of heterogeneous nucleation were mainly carried out on small systems with a relatively small substrate size [3]. Such simulation systems mainly represent the cases for $r_n > r_N$, where the 2D nucleus covers the entire substrate surface (Figure 4(a)). More recently, our MD simulations have been extended to larger systems with a relatively large substrate size. We found that in many cases, the 2D nucleus only covers partially the substrate surface, i.e., $r_n < r_N$ (Figures 4(b) and (c)). Here we choose 2 specific systems to demonstrate these 2 typical scenarios.

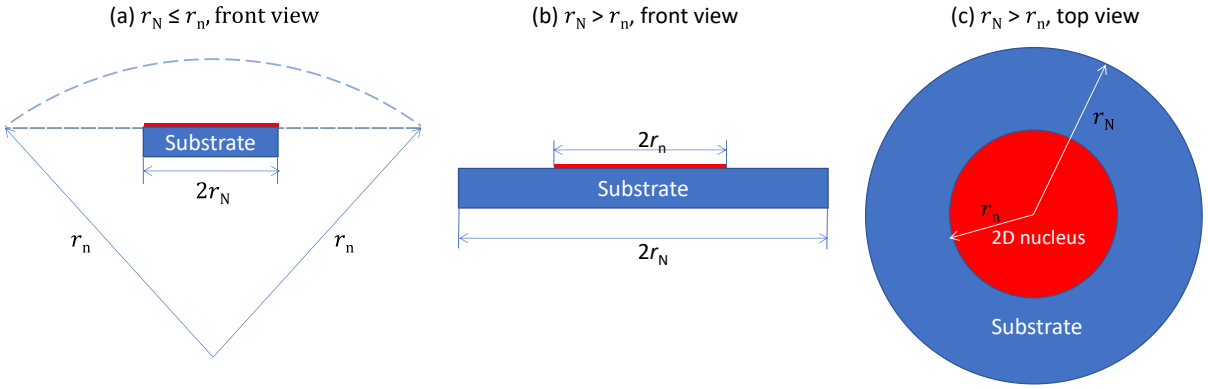

Figure 4. Schematic illustration of substrate size effect on heterogeneous nucleation behaviour. (a) when $r_N \le r_n$ the 2D nucleus covers the entire substrate surface; and (b) when $r_N > r_n$ the 2D nucleus only covers partially the substrate surface, as shown in (c).

We first consider heterogeneous nucleation in the case of $r_N \le r_n$. Figure 5 presents the front view of time-averaged atomic positions of the system and top views of L3 in the simulation system with 2% misfit during heterogeneous nucleation at $\Delta T_n = 40$ K, showing the process of creating the 2D nucleus. The ordered region in L3 extends in size with increasing simulation time and covers the entire substrate surface to provide the 2D nucleus at $t = 1000$ ps, which has the same atomic arrangement as in a perfect {1 1 1} plane of fcc Al. For this system, nucleation occurs at $\Delta T_n = 40$ K (corresponding to $2r_n = 14.1$ nm from Eq. 2) on a substrate of $2r_N = 8.6$ nm (corresponding to $\Delta T_{gi} = 66$ K from Eq. 7), representing a typical case for $r_n > r_N$ as depictured in Figure 4(a).

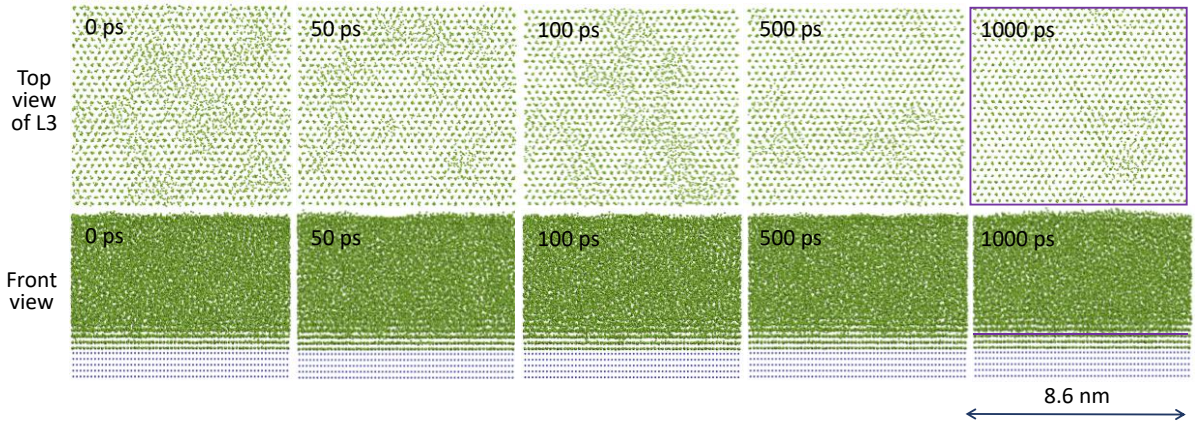

Figure 5. Demonstration of heterogeneous nucleation process in the case of $r_N \le r_n$. Time-averaged atomic positions of a simulation system with 2% lattice misfit showing the evolution of atomic arrangement in the simulation system (front view) and in L3 (the top view) during heterogeneous nucleation process. Nucleation is completed at $t = 1000$ ps to provide a 2D nucleus (L3) which is a crystal plane of the solid (marked in purple). For this system, nucleation occurs at $\Delta T_n = 40$ K ($2r_n = 14.1$ nm) on a substrate of $2r_N = 8.6$ nm ($\Delta T_{gi} = 66$ K).

We now consider heterogeneous nucleation in the case of $r_N > r_n$. Figure 6 shows the nucleation process of a system with -8% lattice misfit demonstrating a typical case for $r_N > r_n$ as depictured in Figure 4(b). At the stage of prenucleation ($t < 0$ ps, see Figure 6(a)), there exist unstable ordered atomic clusters in L3, and a precursor is created at $t = 0$ ps, when one of the ordered atomic clusters becomes stabilized (not to disappear with time) as marked by the red dashed circle in L3 at $t = 0$ ps (Figures 6(b)). During heterogeneous nucleation (Figures 6(b) and (c)), this stabilized cluster grows in size with time to create the 2D nucleus at $t = 40$ ps as marked by the purple dashed circle at $t = 40$ ps. For this system, nucleation occurs at $\Delta T_n = 136$ K ($2r_n = 4.2$ nm) on a substrate of $2r_N = 15.7$ nm (ΔT_{gi}

= 36 K), representing a typical case for $r_n < r_N$ as depictured in Figure 4(b). This is similar to the patch nucleation concept proposed by Turnbull in 1950's [48, 49].

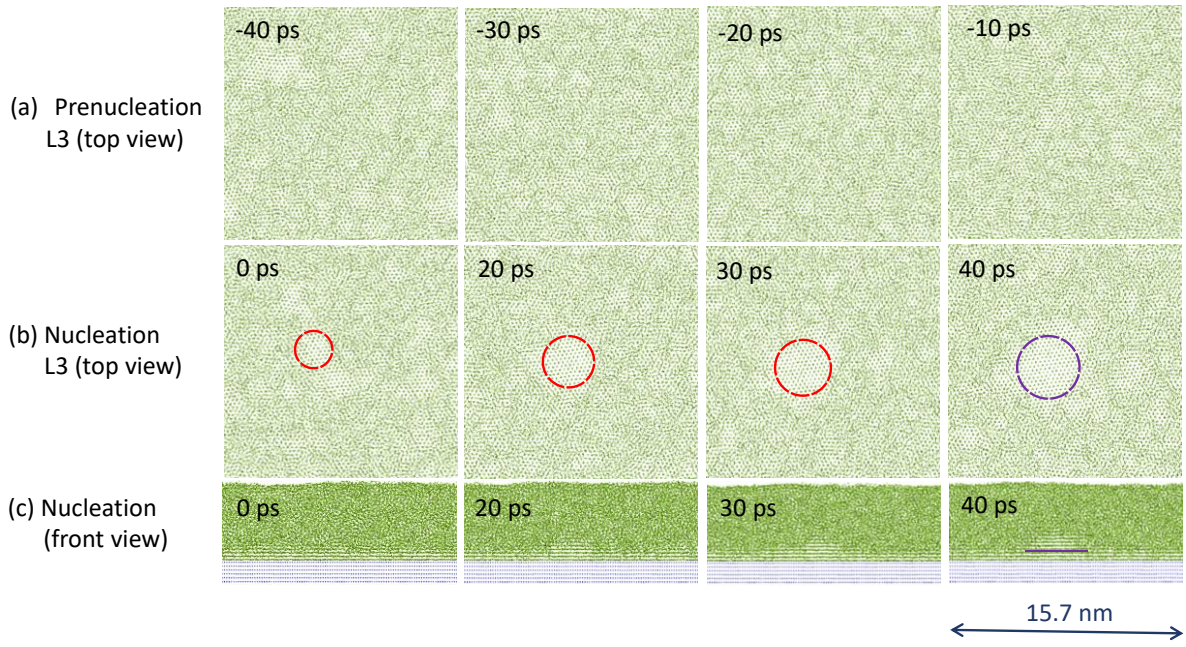

Figure 6. Demonstration of heterogeneous nucleation in the case of $r_N > r_n$. Time-averaged atomic positions of a system with -8% lattice misfit showing the evolution of atomic arrangement in L3 (top view) and in the system (front view) during heterogeneous nucleation process. (a) at prenucleation stage ($t < 0$ ps), there exists dynamically unstable ordered atomic clusters; and (b, c) nucleation occurs at $\Delta T_n = 136$ K, starts at $t = 0$ ps and finishes at $t = 40$ ps to provide a 2D nucleus with $2r_n = 4.2$ nm on a substrate of $2r_N = 15.7$ nm ($\Delta T_{gi} = 36$ K).

Although in the cases of $r_N > r_n$ the 2D nucleus only covers partially the substrate surface, the essential features of heterogeneous nucleation are the same as in the cases where $r_N \leq r_n$, as demonstrated in Figure 7. For the system with 8% misfit, the crystalline lattice in the 2D nucleus has no twist relative to the substrate lattice (Figure 7(a)), while for the system with -8% misfit, the 2D nucleus has a 6° twist relative to the substrate as indicated by the red line (Figure 7(b)).

Figure 8 is a plot of the nucleation undercoolings (ΔT_n) against the radii of the 2D nuclei (r_n) obtained from all the simulations systems conducted in our recent work in comparison with the theoretical predictions by the classical nucleation theory (Eq. 2). It is interesting to note that the MD data agree well with the homogeneous CNT predictions, being particularly well for the data obtained from large simulation systems. The CNT predictions by Eq. 2 are for 3D nuclei (r^*) obtained by homogeneous nucleation while the MD data represent the relationship between ΔT_n and r_n for the 2D nuclei of heterogeneous nucleation. This good agreement in Figure 8 will be discussed further in Section 5.

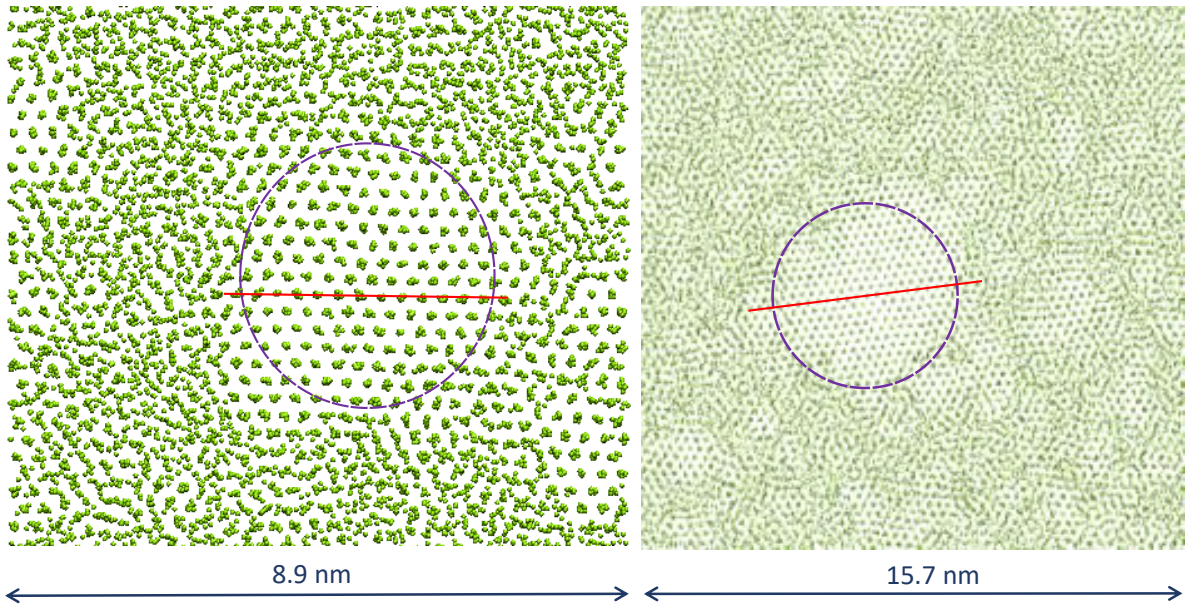

Figure 7. Time-averaged atomic positions in L3 of the simulation systems with (a) 8% lattice misfit; and (b) -8% lattice misfit showing the atomic arrangement in the 2D nuclei relative to that in the substrate. There is no lattice twist in the system with 8% lattice misfit while there is a 6° twist in the system with -8% lattice misfit. The red lines mark the <1 1 0> direction of the 2D nuclei and the <1 1 0> direction of the substrate is parallel to the bottom edge of the images.

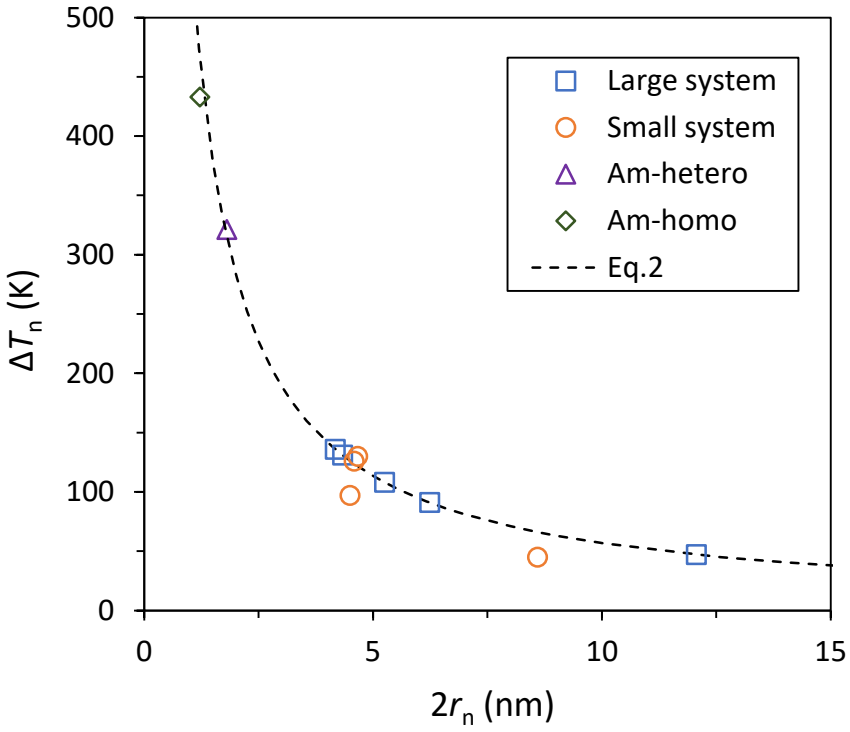

Figure 8. The 2D nucleus size ($2r_n$) obtained in different simulation systems plotted as a function of nucleation undercooling (ΔT_n) in comparison with $2r^*$ predicted by the classical nucleation theory (Eq. 2, the dashed line). The small systems have 5400 atoms; the large systems have about 80000 atoms; "Am-Hetero" denotes heterogeneous nucleation on 2D amorphous substrate; and Am-homo" denotes homogeneous nucleation with the presence of 3D amorphous substrate.

4. Grain initiation on a single substrate

After the 3-layer nucleation, the 2D nucleus will template further growth and the solidification enters the growth stage. However, as discussed in the previous sections, further growth of the 2D nucleus may need to overcome an energy barrier before it can grow isothermally (i.e., grain initiation). This energy barrier originates from structural templating mechanism, in which solid atoms (not liquid atoms) may provide low energy positions for growing the next layer as illustrated in Figure 9. A consequence of structural templating is that the number of atoms in the atomic layers along the growth direction will decrease during the growth. This is how the curvature is developed after nucleation. It is well understood in the literature that curvature will cause constrain to further growth and further undercooling may be required to overcome such constraint [50]. In this section, we use MD simulations to investigate the curvature effect on grain initiation behaviour.

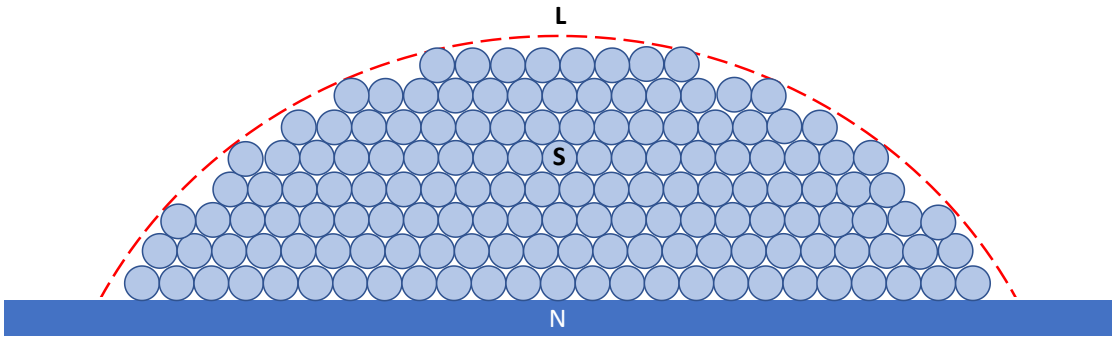

Figure 9. Schematic illustration of curvature formation (the red dashed line) as a consequence of structural templating during formation of a spherical solid cap (S) on a substrate (N) from the liquid (L). Structural templating requires a solid atom to be supported only by solid atoms in the next solid layer underneath it. This means that during both nucleation and growth a new solid layer always contains smaller numbers of atoms than its previous layer.

4.1. Constrained grain initiation

We use MD simulation results obtained from the systems with 2% misfit to demonstrate the concept of constrained grin initiation. It was identified that this system requires a nucleation undercooling of ΔT_n = 40 K to create the 2D nucleus at t = 1000 ps on a substrate of $2r_N$ = 8.6 nm which corresponds to ΔT_{gi} = 66 K (see Figure 5). We observed that no further growth was possible with prolonged simulation time after nucleation. The system was then subjected to increased undercoolings for further growth (Figure 10). It was found that further growth takes the form of spherical caps. For each increase of undercooling, the solid grows quickly to a certain cap height with a specific curvature (r_{LS}, the curvature of the L/S interface) and then becomes stagnant with time. Analogous to Eqs. 2 and 8, one has the following equation for r_{LS}:

$$\Delta T r_{LS} = 2\Gamma, \quad (10)$$

where ΔT is the undercooling required to deliver the dormant cap with a curvature of r_{LS}.

This growth behaviour needs further explanation. After nucleation, further growth will develop curvature which represents a constraint (or energy barrier) to further growth (Figure 9). Further undercooling is required to overcome such curvature constraint. Figure 11(a) schematically illustrates the free energy change during nucleation and further growth for 3 different undercoolings as a function of the total number of solidified atoms with the relative positions of the relevant temperatures being shown in Figure 11(b). As shown in our previous work [3], 3-layer nucleation is a spontaneous down-hill process. However, further growth (e.g., at T_1) leads to the increase in free energy (ΔG) due to the creation of curvature and the ΔG curve has a maximum corresponding to an energy barrier (ΔG^*). Further decrease in temperature (or increase in undercooling) results in a decrease of the energy barrier due to the reduced curvature constraint. At each temperature, the solid and liquid reaches a metastable equilibrium to define the metastable curvature

given by Eq. 2. Thus, for each increase in undercooling there will be some further growth of the cap limited by the new curvature creased under this undercooling (see Figure 11(c)). However, when ΔT reaches ΔT_{gi} the system reaches an equilibrium state, where the driving force for growth (free energy decrease due to solidification) balances the curvature constraint, as described by Eq. 7. When $\Delta T > \Delta T_{gi}$, the system becomes unstable, isothermal growth will be barrierless, and the system enters the free growth stage.

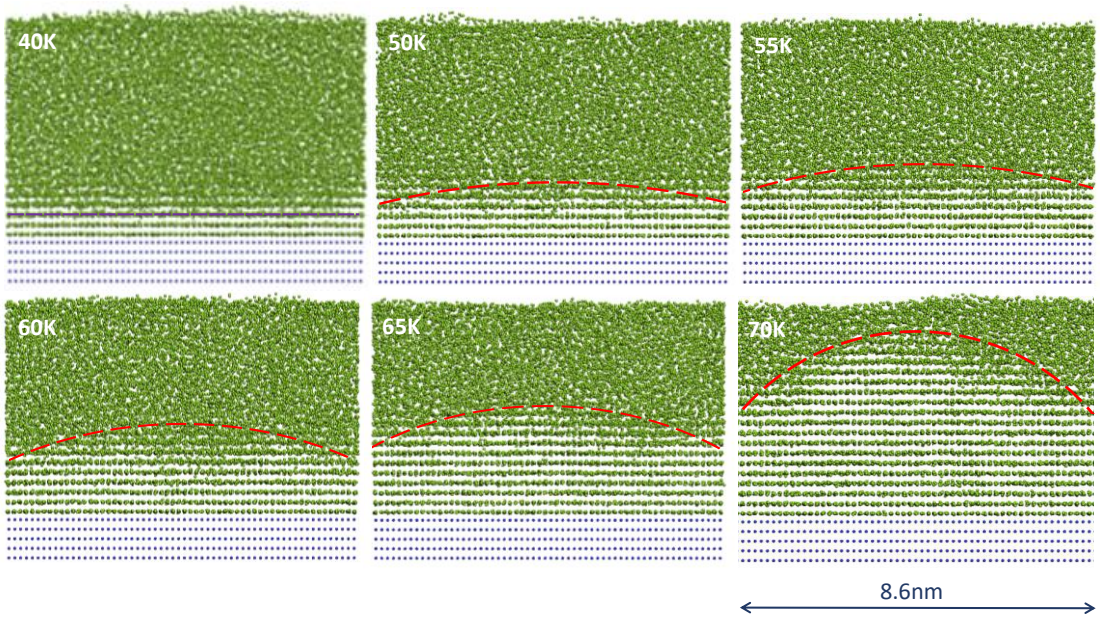

Figure 10. Time-averaged atomic positions of a simulation system with 2% lattice misfit showing the constrained cap formation process. After nucleation at $\Delta T_n = 40$ K, further growth of the solid can only be made possible by increasing the undercooling. For this system, nucleation occurs at $\Delta T_n = 40$ K ($2r_n = 14.2$ nm) on a substrate of $2r_N = 8.6$ nm ($\Delta T_{gi} = 66$ K), and the system was then subject to growth under increased undercooling that is marked by the data on each image.

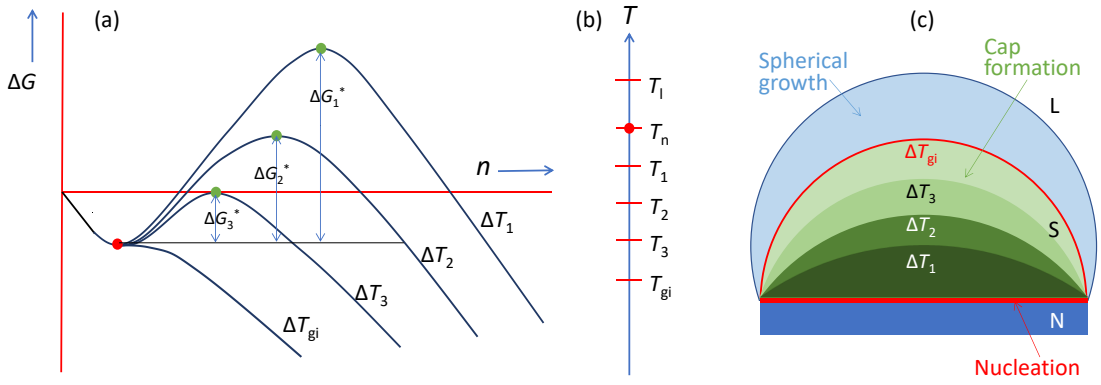

Figure 11. Schematic illustration of the constrained cap formation process. (a) free energy change (ΔG) as a function of the number of solid atoms (n) at different undercoolings (ΔT); (b) relative position of different temperatures (T); and (c) the constrained cap formation process with decreasing temperature. The red dot marks the nucleation finishing point, and the green dots mark the maximum ΔG which defines the energy barrier for free growth at each undercooling.

4.2. Unconstrained grain initiation

In the previous case, nucleation occurs at an undercooling of $\Delta T_n = 40$ K on a substrate with $\Delta T_{gi} = 66$ K. We have concluded that when $\Delta T_n < \Delta T_{gi}$, the spherical cap formation is a constrained growth process in which further growth requires an increase in undercooling to overcome an energy barrier. However, when $\Delta T_n > \Delta T_{gi}$, after nucleation further growth becomes barrierless, and the spherical cap formation becomes an unconstrained

process. In this section, we use MD simulation results to demonstrate such an unconstrained spherical cap formation process.

We turn to the system with 2% misfit again. Heterogeneous nucleation takes place in this system under an undercooling ΔT_n = 40 K to create a 2D nucleus at t = 1000 ps that covers the entire substrate surface (Figure 5), but there is no further growth observed afterwards. The system was then subjected to growth at an undercooling of ΔT = 90 K, which is greater than its grain initiation undercooling (ΔT_{gi} = 66 K). Figure 12 shows the spherical cap formation process under isothermal conditions (ΔT = 90 K) as a function of time. It is interesting to note that instead of growing layer-by-layer, the system grows a spherical cap with a base size corresponding to the 2D nucleus size of $2r_n$ = 6.3 nm. The cap height increases with time under isothermal condition, suggesting that such spherical cap formation is barrierless and hence unconstrained. In addition, Figure 12 suggests that spherical cap formation is a process inherent to crystal growth at a given undercooling and has little to do with the nature of the substrate, since the existence of the 2D nucleus formed at ΔT = 40 K has made no difference to the spherical cap formation process.

Another example of unconstrained spherical cap formation is given in Figure 13. For the system with 8% misfit, the nucleation occurred at ΔT_n = 131 K on a substrate of $2r_N$ = 8.9 nm (ΔT_{gi} = 64 K) to provide a 2D nucleus of $2r_n$ = 4.3 nm marked by the purple dashed circle at t = 40 ps in Figure 13. With increasing time, the 2D nucleus grows isothermally initially into a spherical cap (t = 50 ps) and then hemispheres with increasing radius (t > 60 ps). Due to the large undercooling (or small 2D nucleus size), the spherical cap formation process is rather short (less than 20 ps). An interesting phenomenon observed is that after spherical cap formation (formation of the first hemisphere) further growth takes the form of hemispheres until the radius of the hemisphere reaches that of the substrate.

Similar results were obtained in the system with -8% misfit. Figure 14 shows the growth process in this system after heterogeneous nucleation at t = 40 ps. This system grows faster than the system with 8% misfit (Figure 13). The spherical cap formation process occurs within 10 ps and not even show in the time interval in Figure 14. However, the hemisphere growth process after spherical cap formation is the same in both systems.

Such unconstrained spherical cap formation behaviour can be understood with the help of schematic illustration in Figure 15. When $\Delta T_n > \Delta T_{gi}$, both the nucleation and growth processes become barrierless (Figure 15(a)). In such cases, although the free growth criterion is satisfied early at higher temperature, nucleation and spherical cap formation can only occur isothermally at the nucleation temperature, which is lower than the temperature required for free growth (Figure 15(b)). Solidification under such conditions proceeds isothermally through the following steps without any energy barriers (Figure 15(c)):

1) Heterogeneous nucleation through the 3-layer mechanism to generate 2D nucleus with r_n being defined by the nucleation undercooling (ΔT_n).
2) Barrierless spherical cap formation to create a hemisphere with a radius of r_n.
3) Hemispherical growth with an increasing radius to deliver a hemisphere with $r_{LS} = r_N$.
4) Spherical growth beyond the hemisphere with $r_{LS} > r_N$.

Although the spherical growth in Step 4 was not observed in our MD simulation due to the limited size of the system we used, such spherical growth beyond the hemisphere was indeed observed in the phase-field crystal modelling by Gránásy and co-workers [35] and in super MD simulation systems (over 1 million of atoms) conducted by Fujinaga and Shibuta [36].

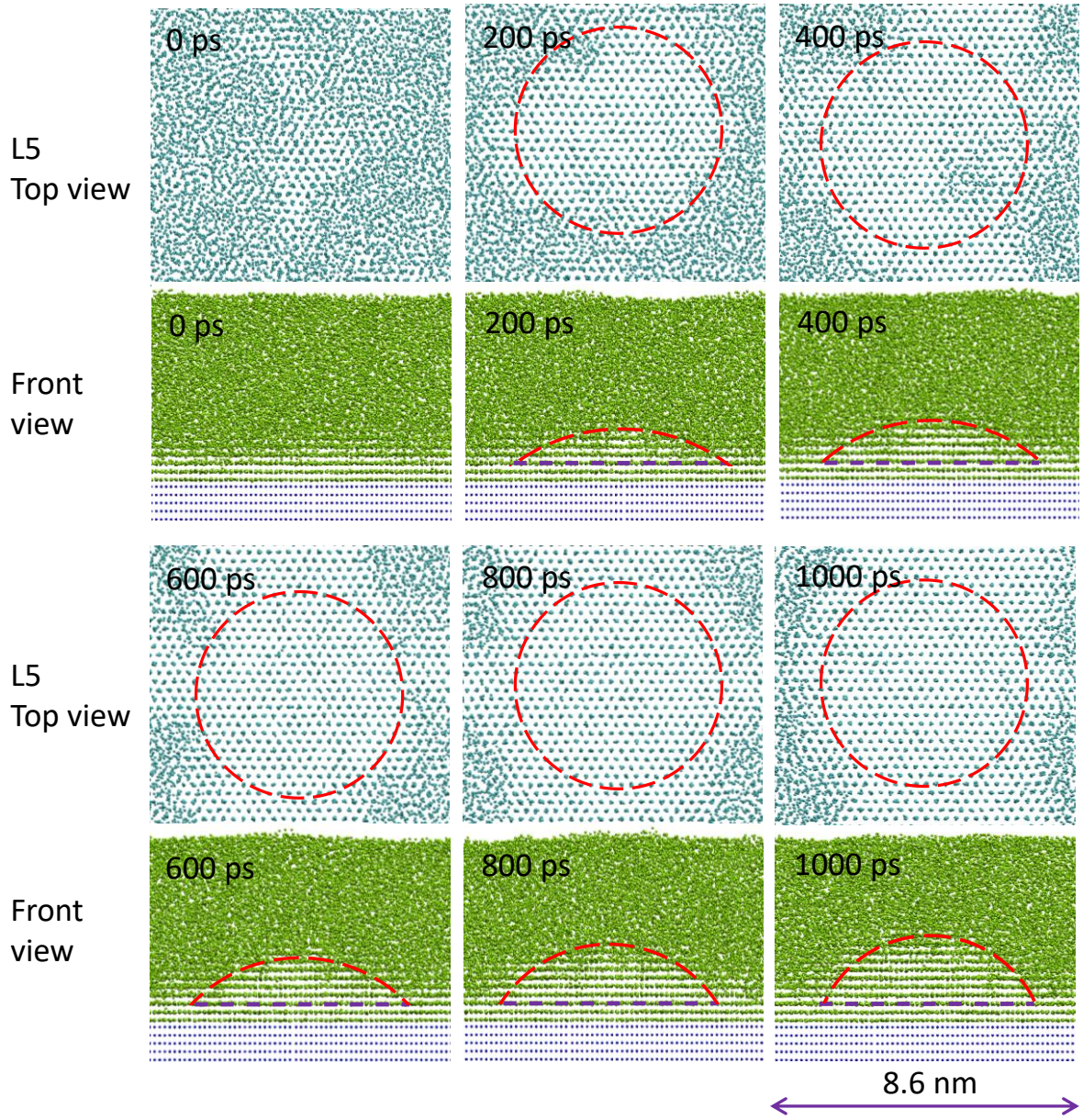

Figure 12. Time-averaged atomic positions of a simulation system with 2% lattice misfit demonstrating the unconstrained cap formation process after nucleation at a higher temperature. Nucleation occurred at $\Delta T_n = 40$ K on a substrate of $2r_N = 8.6$ nm to provide the 2D nucleus that covers the entire substrate surface (see Figure 5). The system was then allowed to solidify at $\Delta T = 90$ K (corresponding to $2r_n = 6.3$ nm as marked by the purple dashed lines in the front views). With increasing time, the 2D nucleus grows into spherical caps with increasing cap height. The top views of L5 are used to demonstrate that the cap grows in height without lateral spreading as shown by the stable size of the crystalline regions indicated by the red circles.

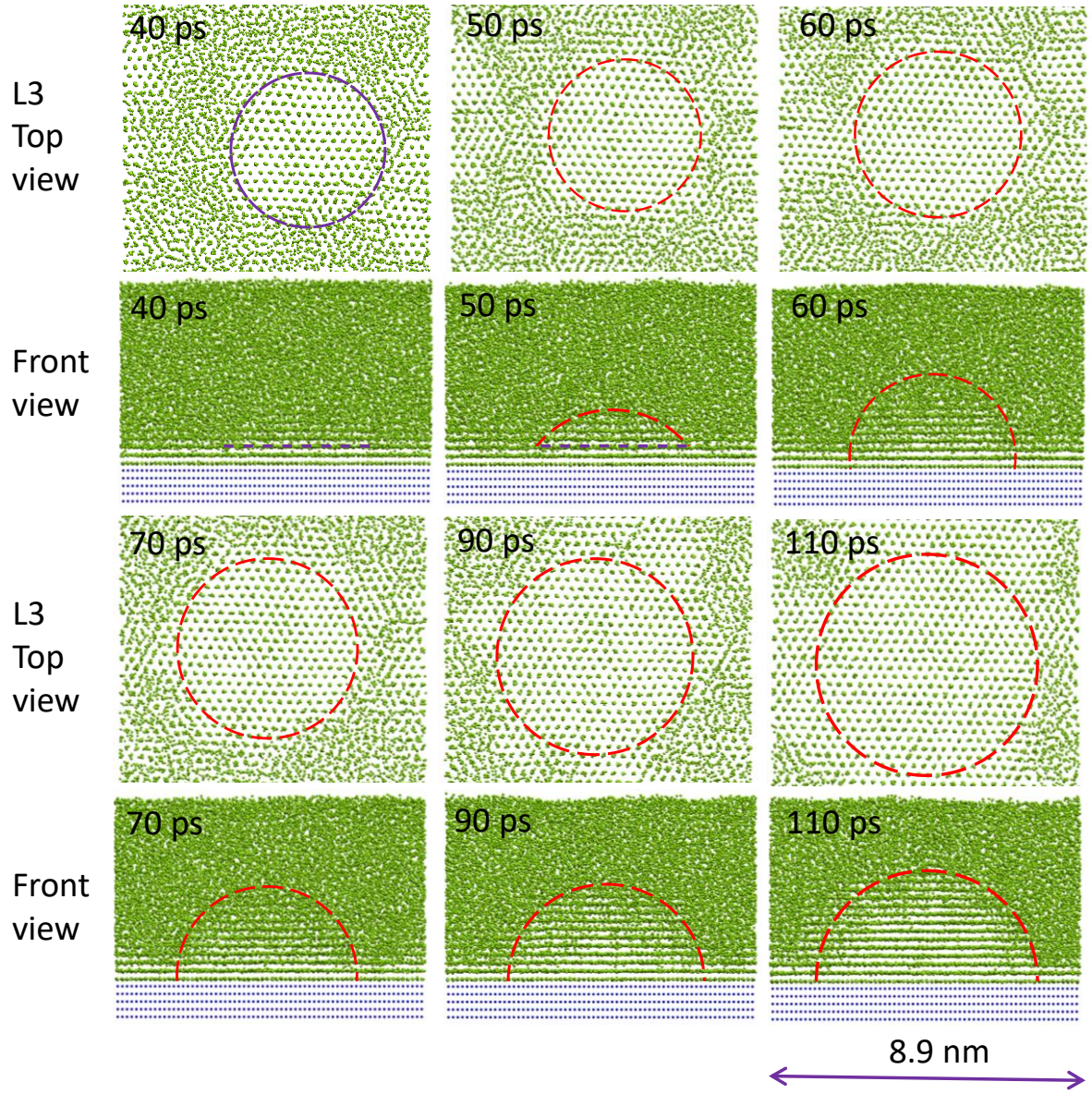

Figure 13. Time-averaged atomic positions of a simulation system with 8% lattice misfit demonstrating the unconstrained cap formation process at a constant temperature. Nucleation occurred at ΔT_n = 131 K on a substrate of $2r_N$ = 8.9 nm to provide the 2D nucleus of $2r_n$ = 4.3 nm (the purple dashed circle at t = 40 ps). With increasing time, the 2D nucleus grows isothermally initially into a spherical cap (t = 50 ps) and then hemispheres with increasing radius (t > 60 ps).

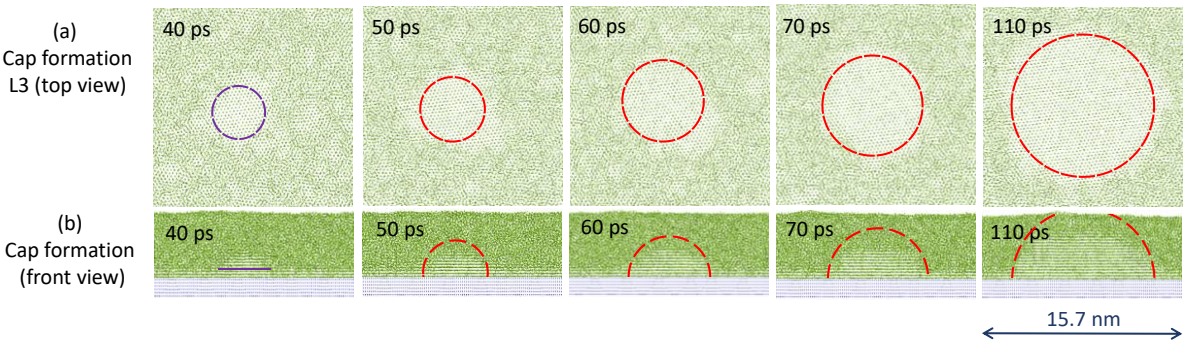

Figure 14. Time-averaged atomic positions of a simulation system with -8% lattice misfit demonstrating the unconstrained cap formation process at a constant temperature. Nucleation occurred at ΔT_n = 136 K on a substrate of $2r_N$ = 15.7 nm (ΔT_{gi} = 36.2 K) to provide the 2D nucleus of $2r_n$ = 4.2 nm (the purple dashed circle at t = 40 ps, see Figure 6)). With increasing

time, the 2D nucleus grows isothermally initially into a spherical cap (40 ps < t < 50ps) and then hemispheres with increasing radius (t > 50ps).

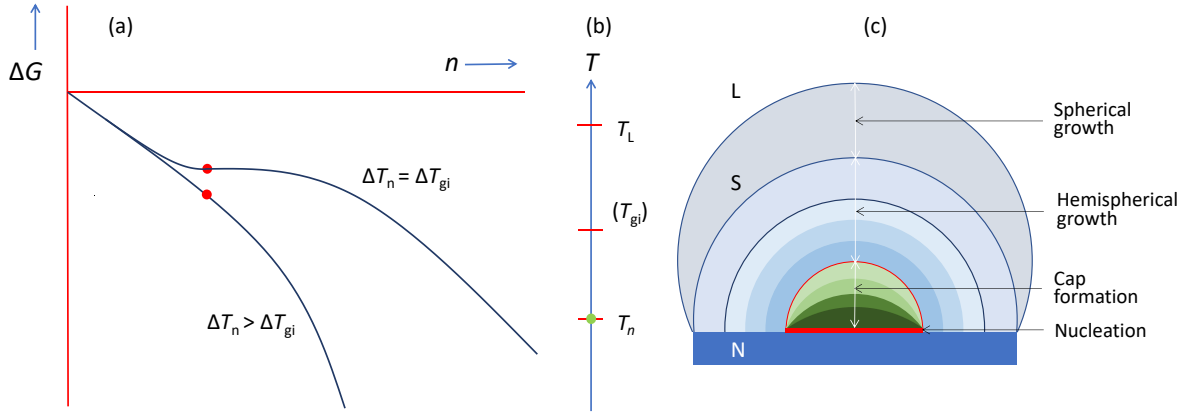

Figure 15. Schematic illustration of the unconstrained cap formation process. (a) free energy change (ΔG) as a function of number of solid atoms (n) at different undercoolings (ΔT); (b) relative position of different temperatures (T); and (c) the unconstrained cap formation process under isothermal condition. The red dot marks the nucleation finishing point. When $\Delta T_n > \Delta T_{gi}$, there is no energy barrier for grain initiation.

4.3. Grain initiation map

Based on our MD simulation results presented previously, it is concluded that grain initiation on a single substrate can be divided into 2 categories: grain initiation through constrained spherical cap formation and grain initiation through unconstrained spherical cap formation. Such grain initiation behaviour is best presented by a grain initiation map (i.e., a ΔT_{gi} - r_N plot), as schematically illustrated in Figure 16. The free growth criterion, $\Delta T_{gi} r_N = 2\Gamma$ (the solid red line), divides the ΔT_{gi} - r_N plot into two zones:

- Zone I: grain initiation through constrained spherical cap formation. Grain initiation in this zone is characterised by $\Delta T_{gi} r_N < 2\Gamma$. Thus, in this zone, we have $\Delta T_n < \Delta T_{gi}$, or equivalently, $r_n > r_N$. The metastable cap formed at a particular temperature is dormant and further growth can only be made possible by increasing the undercooling to overcome the energy barrier.
- Zone II: grain initiation through unconstrained spherical cap formation. Grain initiation in this zone is characterised by $\Delta T_{gi} r_N > 2\Gamma$. Thus, in this zone, we have $\Delta T_n > \Delta T_{gi}$, or equivalently $r_n < r_N$. Grain initiation in this zone becomes barrierless.

5. Modelling of heterogeneous nucleation and grain initiation

5.1. Modelling of heterogeneous nucleation

The heterogeneous nucleation process described in Section 3 starts with a precursor that is the outcome of prenucleation and presented by the L/N interface (6 atomic layers) and finished with 3 layers of solid (L1, L2 and L3) with L3 being the 2D nucleus and a L/S interface (6 atomic layers). This process can be analysed from 2 different angles: (1) free energy change due to increased fraction of solid atoms; and (2) free energy change due to the change in interfacial energies.

From the viewpoint of interfacial energy change, at the nucleation temperature, the free energy change of heterogeneous nucleation (ΔG_n) can be expressed as:

$$\Delta G_n = (\gamma_{SN} + \gamma_{SL} - \gamma_{LN}) n_L A_a \quad (11)$$

where γ_{SN} is the interfacial energy of the S/N interface; γ_{SL} the interfacial energy of the L/S interface; γ_{LN} the interfacial energy of the L/N interface; n_L is the number of atoms in one atomic layer; and A_a is the projected area of an atom. Thus, $n_L A_a$ represents the area covered by the 2D nucleus. For simplicity we assume that at the stage of 3-layer nucleation all 3 interfaces have the same area of $n_L A_a$. This also means that the system under analysis

has 9 atomic layers (3 for the S/N interface and 6 for the S/L interface) between the substrate and the bulk liquid.

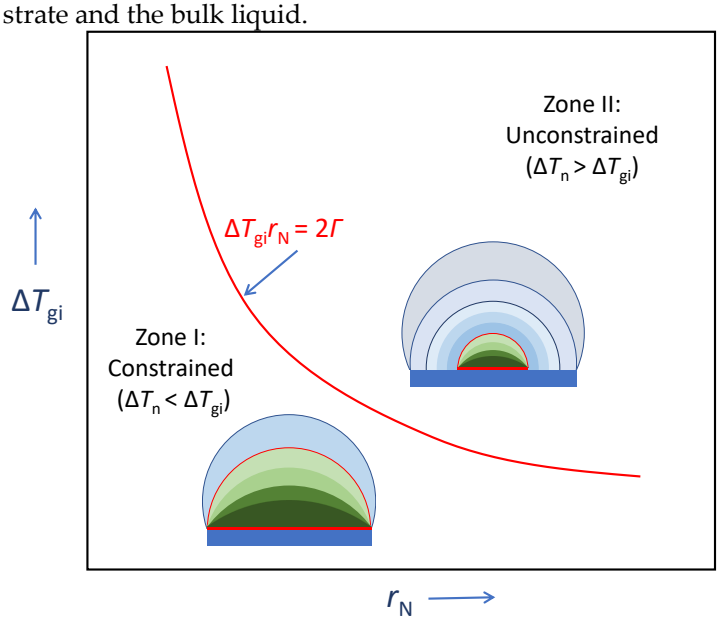

Figure 16. Schematic illustration of grain initiation behaviour on a single substrate. The free growth criterion, $\Delta T_{gi} r_N = 2\Gamma$ (the solid red line), divides the ΔT_{gi} - r_N plot into two regions: I. where $\Delta T_{gi} r_N < 2\Gamma$, grain initiation has an energy barrier and occurs through constrained cap formation; and II. where $\Delta T_{gi} r_N > 2\Gamma$, grain initiation has no energy barrier and occurs through unconstrained cap formation.

From the viewpoint of increase in solid atom fraction during nucleation, ΔG_n can be expressed by the following equation:

$$\Delta G_n = 9 n_L (f_{nf} - f_{ns})(g_S - g_L) \quad (12)$$

where f_{ns} is the solid atom fraction at the starting point of nucleation; f_{nf} the solid atom fraction at the finishing point of nucleation; g_S the free energy per solid atom at T_n; and g_L the free energy per liquid atom at T_n. From Eqs. 11 and 12 we have:

$$(\gamma_{SN} + \gamma_{SL} - \gamma_{LN}) n_L A_a = 9 n_L (f_{nf} - f_{ns})(g_S - g_L) \quad (13)$$

In consideration of $A_a = \pi r^2_a$ and letting $\Delta\gamma = \gamma_{SN} + \gamma_{LS} - \gamma_{LN}$, $\Delta f_s = f_{nf} - f_{ns}$ and $\Delta g = g_s - g_l$, one has:

$$\Delta g = \frac{\pi r_a^2 \Delta\gamma}{9 \Delta f_s} . \quad (14)$$

For pure Al, according to the Pandat Al database [51], Δg can be approximated as a linear function of ΔT (Figure 17):

$$\Delta g = 1.9\text{x}10^{-23} \Delta T_n \text{ (J/atom)} . \quad (15)$$

Considering the volume of an atom $V_a = \frac{4}{3} {r_a}^3$, and $r_a = 1.4$ Å for Al, the free energy change per volume (ΔG_v) is given by the following equation:

$$\Delta G_v = \frac{\Delta g}{V_a} = 1.65\text{x}10^6 \Delta T_n \text{ (Jm}^{-3}\text{)}. \quad (16)$$

Considering the linear relationship in Eq. 15 for Al, ΔG_v can be generally approximated as [52]:

$$\Delta G_v = -\Delta S_v \Delta T \quad (17)$$

where ΔS_v is the entropy of fusion per unit volume. Hence, Eq. 16 suggests that for pure Al $\Delta S_v = 1.65 \times 10^6$ Jm^{-3}K, which is close to 1.112×10^6 Jm^{-3}K, a value frequently used in the literature [28].

In the general cases, combining Eqs. 14, 16 and 17, one has:

$$\Delta T_n = \frac{-\Delta\gamma}{12 \Delta f_s \Delta S_v r_a} . \quad (18)$$

It is important to note that both $\Delta\gamma$ and Δf_s are functions of lattice misfit. Unfortunately, the relevant parameters are not available to test the validity of Eq. 18.

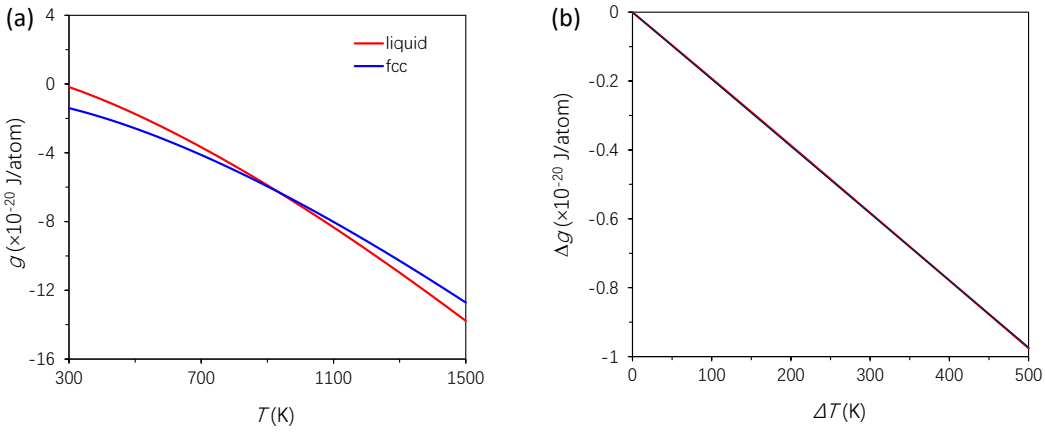

Figure 17. Free energy of pure Al as a function of temperature. (a) free energy per Al atom (g) as a function of temperature (T); (b) free energy change (from liquid to solid) per Al atom (Δg) as a function of undercooling (ΔT). Source data: Pandat Al-DAT [51]. Although free energy of both liquid and solid Al is a non-linear function of temperature (a), the free energy change for solidification is a linear function of undercooling (b).

5.2. *Understanding of grain initiation*

Although grain initiation has been used interchangeably with heterogeneous nucleation in the literature [29], it is distinctively different from heterogeneous nucleation. As will be discussed in depth later, it is not only theoretically desirable but practically beneficial to treat heterogeneous nucleation and grain initiation as two separate processes.

In the literature, grain initiation is well described by the free growth criterion (Eqs. 7 and 8) developed by Greer et al. [28]. Grain initiation on a substrate of r_N is only possible when $\Delta T_{gi} r_N > 2\Gamma$. It is clear from Eq. 8 that grain initiation is about free growing a solid particle and has nothing to do with the substrate except the substrate size (r_N). In this sense, the free growth criterion should be written more appropriately as:

$$\Delta T r_S = 2\Gamma \quad (19)$$

where r_S is the radius of a solid sphere. This means a solid particle with r_S can grow isothermally under an undercooling ΔT if $\Delta T r_S > 2\Gamma$. Replacement of r_S in Eq. 19 by r_N in Eq. 8 has made it possible for grain size prediction, but Eq. 8 is only applicable to the case of constrained spherical cap formation.

Here we offer some further insights of the difference between heterogeneous nucleation and grain initiation:

- ΔT_{gi} is a physical property of a substrate of r_N when $\Delta T_n < \Delta T_{gi}$. However, when $\Delta T_n > \Delta T_{gi}$, Eq. 8 is no longer applicable. In this case, the grain initiation criterion becomes $\Delta T_n r_n = 2\Gamma$. Grain initiation becomes possible when $r_N > r_n$.
- $\Delta T_{nh} r^* = 2\Gamma$ vs. $\Delta T_n r_n = 2\Gamma$ vs. $\Delta T_{gi} r_N = 2\Gamma$: It is important to realise that $\Delta T_{nh} r^* = 2\Gamma$ describes the homogeneous nucleation process (3D), $\Delta T_n r_n = 2\Gamma$ describes the 3-layer nucleation process (2D) while $\Delta T_{gi} r_N = 2\Gamma$ describes the hemisphere formation (3D) on a substrate of r_N, as depictured in Figure 18. The origin of the similarity between these equations is that they all describe balancing the volume free energy change with change in interfacial energies.
- Grain initiation is about free growing isothermally a solid particle which is not directly connected to physical properties of the substrate, while heterogeneous nucleation is dictated by the physical properties of the substrate.

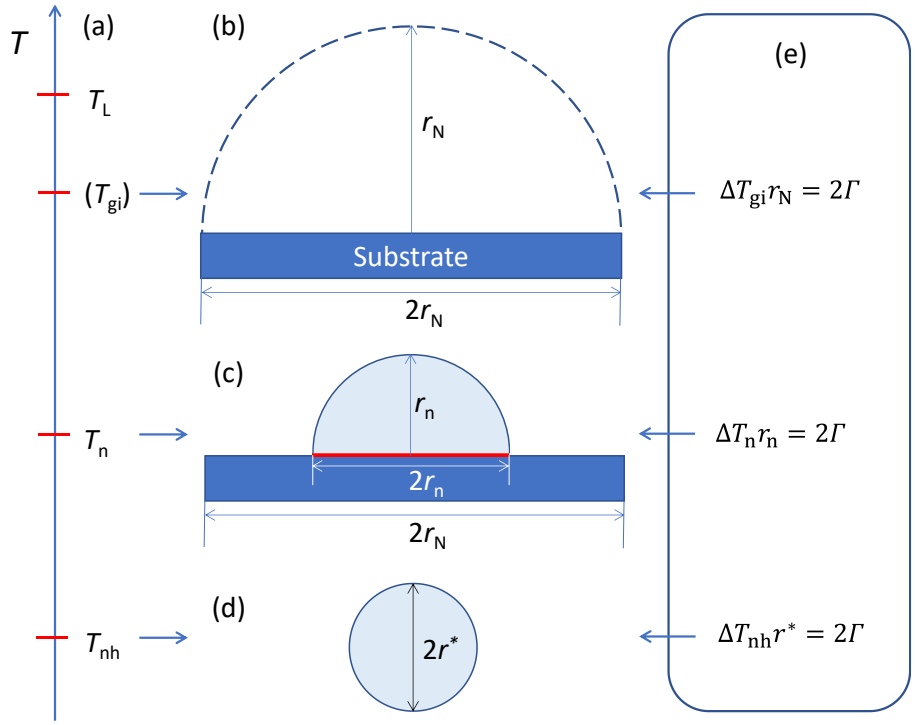

Figure 18. Schematic illustration of the relationships between grain initiation, heterogeneous nucleation and homogeneous nucleation. (a) relative positions of the relevant temperatures; (b) constrained grain initiation; (c) heterogeneous nucleation and unconstrained grain initiation; (d) homogeneous nucleation; and (e) the corresponding governing equations. The dark blue rectangles represent substrates; the red rectangle is 2D nucleus; and the light blue circles denote the solid.

6. Summary

Upon realising that heterogeneous nucleation and grain initiation are two distinctively different processes, we have investigated the grain initiation behaviour on a single substrate with MD simulations. Our MD simulation results have revealed a complex grain initiation behaviour. When $\Delta T_n < \Delta T_{gi}$, spherical cap formation is constrained by the curvature of the L/S interface, a spherical cap is dormant and further growth requires an increase in undercooling to overcome an energy barrier; and grain initiation occurs only when the spherical cap grows beyond the hemisphere. However, when $\Delta T_n > \Delta T_{gi}$, spherical cap formation becomes an unconstrained process, which can proceed isothermally without an energy barrier. Grain initiation through unconstrained spherical cap formation has 3 distinctive stages: (1) spherical cap formation to deliver a hemisphere of radius r_n on the 2D nucleus; (2) hemispherical growth to laterally spread the solid over the substrate surface to eventually provide a hemisphere with radius of r_N; and (3) spherical growth with a curvature beyond r_N.

Our analysis has revealed that homogeneous nucleation (r^*), heterogeneous nucleation (r_n) and grain initiation (r_N) all follow the same form of governing equations ($\Delta Tr = 2\Gamma$). The physical origin for this interesting coincidence is the fact that all these 3 processes are consequences of balancing the volume free energy and the interfacial free energy but at different levels of undercooling. This offers the potential to bridge the atomistic mechanisms for heterogeneous nucleation and grain initiation with the classical nucleation theory.

In addition, through further analysis and discussions, we can provide the following additional new insights into solidification processes:

- Substrate wetted completely by the liquid can always induce some ordered atoms in the liquid adjacent to the liquid/substrate interface and hence can act as nucleation site regardless the nucleation undercooling. Under such conditions, we have $\gamma_{LN} \geq \gamma_{SN}$

+ γ_{LS}, suggesting that the Young's equation (Eq. 4) is inapplicable to any cases for heterogeneous nucleation. Therefore, describing heterogeneous nucleation as a spherical cap formation process may not be a useful approach, since it masks some critical phenomena, such as prenucleation, formation of 2D nucleus and constrained/unconstrained spherical cap formation.

- As a theoretical model, homogeneous nucleation theory that describes a stochastic process for creation of nucleus is conceptually simple and mathematically rigorous. However, it is challengeable to extend homogeneous nucleation theory to heterogeneous nucleation which is a deterministic process. At least classical heterogeneous nucleation theory has not been helpful to generate much useful new insight except the reduction of nucleation barrier by the substrate.
- The basic atomistic mechanism for both heterogeneous nucleation and crystal growth is structural templating, which requires that any solid atom needs to be supported by the solid atoms in the layer underneath it. This fact has made us realise that curvature formation is a consequence of structural templating.

Author Contributions: Z.F. conducted conceptualization of the research, development of the research approach, funding acquisition, supervision and original draft writing; H.M. conducted MD simulations and visualization, and all the authors contributed to review and editing of the manuscript.

Funding: This work has been funded by the EPSRC of the UKRI under the grant number EP/N007638/1.

Data Availability Statement: All data is available in the main text.

Conflicts of Interest: The authors declare no conflict of interest.

References:

1. Kelton, K.F.; Greer, A.L. *Nucleation in condensed mater: Applications in materials and biology.* Pergamon: Oxford, 2010.
2. Kashchiev, D. *Nucleation: Theory with applications.* Butterworth-Heinemann: Oxford, 2000.
3. Fan, Z.; Men, H.; Wang, Y.; Que, Z.P. A new atomistic mechanism for heterogeneous nucleation in the systems with negative lattice misfit: Creating a 2D template for crystal growth. *Metals* **2021**, *11*, 478.
4. Gibbs, J.W. On the equilibrium of heterogeneous substances. *Am. J. Sci.* **1879**, *16*, 441-458.
5. Volmer M.; Weber, A.Z. Nucleus formation in supersaturated systems. *Zeitschrift für Physikalische Chemie* **1926**, *119*, 277-301.
6. Becker R.; Döring, W. Kinetic treatment of nucleation in supersaturated vapors. *Ann. Phys. (Leipzig)* **1935**, *24*, 719-752.
7. Zeldovich, J.B. On the theory of new phase formation. Cavitation. *Acta Physicochimica USSR* **1943**, *18*, 1-22.
8. Cantor, B. Heterogeneous nucleation and adsorption. *Philos. Trans. R. Soc. Lond.* **2003**, *361*, 409-417.
9. Kim, W.T.; Zhang, D.L.; Cantor B. Nucleation of solidification in liquid droplets. *Metall. Trans. A* **1991**, *22A*, 2487-2501.
10. Kim, W.T.; Cantor, B. Solidification of tin droplets embedded in an aluminium matrix. *J. Mater. Sci.* **1991**, *26*, 2868-2878.
11. Kim, W.T.; Cantor, B. Solidification behaviour of Pb droplets embedded in a Cu matrix. *Acta Metall.* **1992**, *40*, 3339-3347.
12. Kim, W.T.; Cantor, B. Heterogeneous nucleation of Al_2Cu in Al-Cu eutectic liquid droplets embedded in an Al matrix. *Acta Metall. Mater.* **1994**, *42*, 3045-3053.
13. Stranski, I.; Kaischew, R. Über den mechanismus des gleichgewichtes kleiner kriställchen I. *Z. Phys. Chem. B* **1934**, *26*, 100-113.
14. Richards, WT. The persistence and development of crystal nuclei above the melting temperature. *J. Am. Chem. Soc.* **1932**, *54*, 479-495.
15. Coudurier, L.; Eustathopoulos, N.; Desré, P.; Passerone, A. Rugosite atomique et adsorption chimique aux interfaces solide-liquide des systems metalliques binaires. *Acta Metall.* **1978**, *26*, 465-475.
16. Cantor, B. Embedded droplet measurements and an adsorption model of the heterogeneous nucleation of solidification. *Mater. Sci. Eng. A* **1994**, *178*, 225-231.
17. Kim, W.T.; Cantor, B. An adsorption model of the heterogeneous nucleation of solidification. *Acta Metall. Mater.* **1994**, *42*, 3115-3127.
18. Jones, G.P. In: *Solidification technology in the foundry and cast house*. London: The Metals Society; 1983. p. 112-114.
19. Jones, G.P. In: Beech J, Jones H, editors. *Solidification processing 1987*. London: The Institute of Metals; 1988. p. 496-499.
20. Fan, Z.; Wang, Y.; Zhang, Y.; Qin, T.; Zhou, X.R.; Thompson, G.E.; Pennycook, T.; Hashimoto. T. Grain refining mechanism in the Al/Al-Ti-B system. *Acta Mater.* **2015**, *84*, 292-304.
21. Wang, Y.; Fang, C.M.; Zhou, L.; Hashimoto, T.; Zhou, X.; Ramasse, Q.M.; Fan, Z. Mechanism for Zr poisoning of Al-Ti-B based grain refiners. *Acta Mater*. **2019**, *164*, 428-439.
22. Wang, Y.; Que, Z.P.; Hashimoto, T.; Zhou, X.R.; Fan, Z. Mechanism for Si poisoning of Al-Ti-B grain refiners in Al alloys. *Metall. Mater. Trans. A* **2020**, *51*, 5743-5757.
23. Wang, S.H.; Wang, F.; Wang, Y.; Ramasse, Q.M.; Fan, Z. Segregation of Ca at the Mg/MgO interface and its effect on grain refinement of Mg alloys. *IOP Conf. Series: Materials Science and Engineering* **2019**, *529*, 012048.
24. Fan, Z.; Wang, SH.; Niu, Z.C. Modification of γ-Al2O3/Al interface through La interfacial segregation: a strategy to harness native γAl2O3 for grain refinement. **2002**, (submitted to *Acta Mater.*)

25. Men, H.; Fan, Z. Prenucleation induced by crystalline substrates. *Metall. Mater. Trans. A* **2018**, *49*, 2766-2777.
26. Fan, Z.; Men, H. A molecular dynamics study of heterogeneous nucleation in generic liquid/substrate systems with positive lattice misfit. *Mater. Res. Express* **2020**, *7*, 126501.
27. Men, H.; Fan, Z. Heterogeneous nucleation mechanisms in systems with large lattice misfit demonstrated by the Pb(*l*)/Cu(*s*) system. *Metals* **2022,** in this special issue.
28. Greer, A.L.; Bunn, A.M.; Tronche, A.; Evans, P.V.; Bristow, D.J. Modelling of inoculation of metallic melts: application to grain refinement of aluminium by Al-Ti-B. *Acta Mater.* **2000**, *48*, 2823-2835.
29. Quested, T.E.; Greer, A.L. Athermal heterogeneous nucleation of solidification. *Acta Mater.* **2005**, *53*, 2683-2692.
30. Quested, T.E.; Greer, A.L. The effect of the size distribution of inoculant particles on as-cast grain size in aluminium alloys. *Acta Mater.* **2004**, *52*, 3859-3868.
31. Shu, D.; Sun, B.D.; Mi, J.; Grant, P.S. A quantitative study of solute diffusion field effects on heterogeneous nucleation and the grain size of alloys. *Acta Mater.* **2011**, *59*, 2135–2144.
32. Du, Q.; Li, Y.J. An extension of the Kampmann–Wagner numerical model towards as-cast grain size prediction of multicomponent aluminium alloys. *Acta. Mater.* **2014**, *71*, 380-389.
33. Men, H.; Jiang, B.; Fan, Z. Mechanisms of grain refinement by intensive shearing of AZ91 alloy melt. *Acta Mater.* **2010**, *58*, 6526-6534.
34. Men, H.; Fan, Z. Effects of solute content on grain refinement in an isothermal melt. *Acta Mater.* **2011**, *59*, 2704-2712.
35. Tóth, G.I.; Tegze, G.; Pusztai, T.; Gránásy, L. Heterogeneous crystal nucleation: The effect of lattice mismatch. *Phys. Rev. Lett*. **2012**, *108*, 025502.
36. Fujinaga, T.; Shibuta, Y. Molecular dynamics simulation of athermal heterogeneous nucleation of solidification. *Comput. Mater. Sci*. **2019**, *164*, 74-81.
37. Fan, Z. An epitaxial model for heterogeneous nucleation on potent substrates. *Metall. Mater. Trans. A* **2013**, *44*, 1409-1418.
38. Fan, Z.; Men, H. An overview of recent advances on understanding of atomistic mechanisms of heterogeneous nucleation. *Metals* **2022,** in this special issue.
39. Fan, Z.; Gao, F.; Jiang B.; Que, Z.P. Impeding nucleation for more significant grain refinement. *Scientific Reports* **2020**, *10*, 9448
40. Fan, Z.; Gao, F. Grain initiation and grain refinement: An overview. *Metals* **2022,** in this special issue.
41. Fang, C.M.; Men, H.; Fan, Z. Effect of substrate chemistry on prenucleation. *Metall. Mater. Trans. A* **2018**, *49*, 6231-6242.
42. Jiang, B.; Men, H.; Fan, Z. Atomic ordering in the liquid adjacent to an atomic-level rough substrate surface. *Comput. Mater. Sci*. **2018**, *153*, 73-81.
43. Zope, R.R; Mishin, Y. Interatomic potentials for atomistic simulations of the Ti-Al system. *Phys. Rev. B* **2003**, *68*, 024102.
44. Todorov, I.T.; Smith, W.; Trachenko, K.; Dove, M.T. Interatomic potentials for atomistic simulations of the Ti-Al system. *J. Mater. Chem*. **2006**, *16*, 1911-1918.
45. Jackson, K.A. The interface kinetics of crystal growth processes. *Interface Sci.* **2002**, *10*, 159-169.
46. Steinhardt, P.J.; Nelson, D.R.; Ronchetti, M. Bond-orientational order in liquids and glasses. *Phys. Rev. B* **1983**, *28*, 784-805.
47. Baumgartner, J.; Dey, A.; Bomans, P.H.H.; Coadou, C.L.; Fratzl, P.; Sommerdijk, N.A.J.M.; Faivre, D. Nucleation and growth of magnetite from solution. *Nat. Mater*. **2013**, *12*, 310-314.
48. Turnbull, D. Kinetics of solidification of supercooled liquid mercury droplets. *J. Chem. Phys.* **1952**, *20*, 411-424.
49. Turnbull, D. Theory of catalysis of nucleation by surface patches. *Acta Metall.* **1953**, *1*, 8-14.
50. Kurz, W.; Herlach, D.M. *Solidification and crystallization*, Wiley, 2006.
51. Pandat with Pan Al database (www.computherm.com).
52. Boettinger, W.J.; Banerjee, D.K. Solidification. In Physical Metallurgy, 5th ed.; Laughlin, D., Hono, K., Eds.; Elsevier Science & Technology: Amsterdam, The Netherlands, 2014; p. 667.